

Extraction of Motion Artifacts from the Measurements of a Wireless Electrocardiogram using Tensor Decomposition

Jannis Lilienthal

*Institute of Software and Multimedia Technology
Technische Universität Dresden
01062 Dresden, Germany
jannis.lilienthal@tu-dresden.de*

Waltenegus Dargie

*Institute of Software and Multimedia Technology
Technische Universität Dresden
01062 Dresden, Germany
waltenegus.dargie@tu-dresden.de*

Abstract—Wireless electrocardiograms facilitate long-term and affordable monitoring of patients in their residential and work environments. However, the measurements are often affected by motion artifacts whose statistical properties are difficult to model or estimate. In this paper we employ tensor decomposition to model motion artifacts. Our approach is based on two steps. Firstly, we transform the ECG measurements into time-frequency space using the continuous wavelet transform and construct a three-dimensional array (the wireless ECG provides three different channels and the wavelet transform of each channel generates a two-dimensional matrix encoding spectral and temporal aspects). Secondly, we employ tensor decomposition to factorize the data and extract motion patterns. We consider different types of movements associated with everyday activities and validate our method by comparing the correlation between the motion artifacts we establish with inertial measurements which are taken in sync with the ECG measurements.

Index Terms—Tensor decomposition, motion artifact, artifact extraction, wireless electrocardiogram, telemedicine, inertial sensor, bio-medical signal processing

I. INTRODUCTION

According to the latest statistics revealed by the World Health Organization (WHO), cardiovascular diseases (CVD) accounted for 17.9 million deaths worldwide in 2016 [1]. With a share of 31% in all global deaths, CVD are the leading causes of death. Within the European Region, CVD cause more than half of all deaths.

People with cardiovascular diseases need early detection and management to reduce mortality risk. The electrocardiogram (ECG) measures the hearts' electrical activities on the surface of the body and reveals potential pathological conditions. In this respect, the availability of affordable and reliable electrocardiograms is crucial for the early diagnosis of CVD. Various wireless electrocardiograms have been developed by several companies and the research community [2]–[6]. One of the challenges of employing these devices in real life is that the free movement of patients generates a significant amount of motion artifacts which can hinder the accurate interpretation

of the ECG signals. Existing or proposed approaches deal with artifacts mainly in two ways: (1) Discarding segments which are subject to noise or (2) filtering out the useful ECG measurement. As to the former, the discarded segments may contain useful pathological symptoms. As to the second, a method to extract the vital signal component needs to be available. Since motion artifacts and cardiac activities show significant overlap in frequency spectrum [7], conventional frequency filters, such as butterworth bandpass filters, fail to separate them.

In the past, advanced filtering techniques have been proposed, including independent component analysis [8], [9], adaptive filters [10], [11], wavelet transformation [12], [13], as well as a combination of some of these [14], [15]. In this paper, we propose a dimensionality reduction technique to model and reason about motion artifacts. Thus, using a wireless ECG, we measure cardiac action potentials while a subject undertakes different types of physical activities. These activities generate and superimpose motion artifacts. Simultaneously, we deploy inertial sensors to measure the rectilinear and curvilinear accelerations produced by the physical activities. Finally, we set up a tensor and apply tensor decomposition in order to uncover hidden motion patterns which can be regarded as motion artifacts.

The remaining part of this paper is organized as follows: In Section II we review related work. In Section III we give a brief overview of matrix factorization methods and an introduction to tensor decomposition. In Section IV we describe our experimental setup, including the ECG and inertial measurements, and our concept for tensor decomposition. In Section V we discuss the results of our signal decomposition approach. Closing with Section VI, we conclude our work and state open issues that we wish to target in future research.

II. RELATED WORK

Our review of related work focuses on the application of advanced processing techniques, including tensor decomposition, on bio-medical signals.

Romero et al. [14] applied independent component analysis (ICA) and principal component analysis (PCA) in order to reduce motion artifacts in ECG. They collected clean ECG signals from subjects at rest. By placing electrodes on the subjects back, they tried to record motion artifacts with negligible influence of cardiac action potentials. These artifacts were superimposed on the clean ECG to obtain noisy segments. Each motion artifact signal was multiplied by a gain factor in order to achieve a specific signal-to-noise ratio (SNR) between 10 dB and -10 dB. Performance evaluation of the method was carried out by comparing the results of a beat detection algorithm from unfiltered vs. filtered signals. The results indicate that both PCA and ICA increase the beat detection accuracy for all SNR values compared to unfiltered signals. Disadvantages of this method are the local offset between the location where the artifacts were recorded and the ECG and generating artificial artifacts.

Kline et al. [16] investigated an experimental method to isolate motion artifacts in electroencephalogram (EEG). By insulating subjects' scalps with swimming caps, they blocked all electrophysiological signals. A wig coated with conductive gel was used to simulate an electrically conductive scalp on the swimming cap. To investigate the correlation between motion artifacts recorded and motion patterns performed they mounted an accelerometer on the head. Nine subjects were walking on a treadmill at different speeds to induce motion artifacts of varying degree. They report that motion artifacts were recorded by the EEG electrodes but show substantial variation across speed, subject, and electrode location. Thus, the researchers were unable to establish a correlation between accelerometer measurements and motion artifacts present in EEG data.

Acar et al. [17] employed tensor decomposition to differentiate between artifacts and epileptic seizures in EEG recordings. Their study included ictal EEG from seven patients subject to ten seizures in total. The researchers constructed an epilepsy tensor by applying time-frequency analysis (Continuous Wavelet Transform, CWT) on multichannel EEG, resulting in a multi-way array of dimensions $time \times scale \times electrode$. Their objective was to identify spatial artifact sources (e.g. eye blink artifact or muscle artifact) and an epileptic activity generating a seizure. They implemented a tensor decomposition model (canonical polyadic decomposition, CPD) which was used to identify patterns indicative of artifacts. By this means, the model was able to localize a seizure origin making use of the spatial dimension of the tensor (EEG electrodes). Moreover, they were able to extract artifacts from EEG recordings using CPD, matching time and location of visually identified artifacts by neurologists. By this means spectral properties of an artifact were analyzed emphasizing that most artifacts feature low-frequency content. Lastly, they used higher order tensor decomposition to remove artifacts such as eye movements from the EEG data, in cases where artifacts account for most of the variation during an ictal period and seizures cannot be decomposed by CPD. They employ Tucker tensor decomposition to decompose the data, remove artifacts and construct a new, artifact reduced, dataset.

Dargie [18] established the motion artifact statistics for a wireless electrocardiogram by employing linear least mean square estimation. ECG and 3D accelerometer measurements were taken from a healthy subject performing a series of activities. The author established a correlation between the measurements of the inertial sensor and the motion artifacts by considering the interval between T-wave and the P-wave as reference. He constructed the motion artifact statistics from these segments and correlated them with the inertial data.

Billiet et al. [19] utilized tensors to recognize physical activities. They employed a single accelerometer attached to the arm to capture patients' movements. Their approach is based on two parts. Firstly, activities are segmented and matched to similar patterns. Secondly, they construct a tensor by utilizing the two-channel accelerometer data, and the corresponding activity pattern. The resulting tensor spans the dimensions $time \times channel \times activity$. Data features, distinct for certain activities, are extracted by applying higher order discriminant analysis - involving tucker decomposition. Finally, a random forest algorithm serves as a classifier to assign the data to one of the provided activity classes.

To our knowledge, tensor decomposition has rarely been applied to ECG data. Existing approaches focus on characterizing heartbeats. The application on EEG data is more prevalent and artifact extraction has already been conducted successfully.

III. BACKGROUND

Since tensor decomposition methods are often a generalization of matrix decomposition, first we will briefly explain decomposition concepts for the two-dimensional case and then introduce tensor decomposition approaches.

A. Matrix Factorization

A matrix factorization refers to the factorization of a matrix into a product of smaller matrices. Their implementations are often used to extract latent information inherent in the data or as a tool for dimensionality reduction. For example, the singular value decomposition (SVD) decomposes a given matrix \mathbf{X} with dimensions $m \times n$ into the product of three matrices \mathbf{U} , $\mathbf{\Sigma}$ and \mathbf{V} .

$$\mathbf{X} = \mathbf{U}\mathbf{\Sigma}\mathbf{V}^T \quad (1)$$

where \mathbf{U} is the left singular matrix of dimension $m \times r$, $\mathbf{\Sigma}$ is an $r \times r$ non-negative diagonal matrix and \mathbf{V} is the corresponding right singular matrix of dimensions $r \times n$. The columns of \mathbf{U} and \mathbf{V} are orthonormal. One of the essential properties of SVD is the structure of $\mathbf{\Sigma}$. The diagonal entries of this matrix are arranged in descending order of the singular values σ_{ii} (refer to Equation 2). The singular values encode how many basis factors (features) are hidden in the original matrix \mathbf{X} .

$$\sigma_{11} \geq \sigma_{22} \geq \dots \geq \sigma_{\min(mn)} \quad (2)$$

By analyzing the singular values in $\mathbf{\Sigma}$ a low-rank approximation of \mathbf{X} can be identified. Also, the singular values are related to the matrix rank – this is particularly notable when we consider the rank of a tensor decomposition later on. The

rank of the decomposed matrix \mathbf{X} can be determined by the number of singular values in Σ which are zero.

$$\mathbf{X} \approx \sum_{r=1}^R \sigma_{rr} \mathbf{u}_r \circ \mathbf{v}_r \quad (3)$$

The decomposition of \mathbf{X} can also be considered as the outer product of the left and right singular vectors. In other words, SVD decomposes the original matrix \mathbf{X} into a summation of R rank-one matrices, as can be seen in Figure 1.

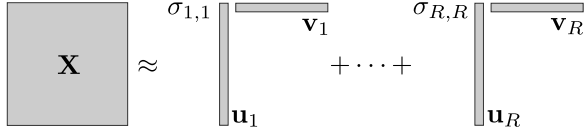


Fig. 1. The principle of Singular Value Decomposition.

The application of singular value decomposition is limited to the two-dimensional data. As we deal with multi-channel ECG, these dimensions are time and channel. However, this would restrain us on the temporal analysis and might hinder the detection of hidden features in the frequency space. As we wish to preserve both – time and frequency aspects – advanced processing techniques are inevitable to handle three-dimensional data.

B. Canonical Polyadic Decomposition

In the following, we will provide a brief introduction into multi-dimensional decomposition methods. In particular, we will explain the canonical polyadic decomposition (CPD), which is considered to be a natural extension of SVD for high-order tensor spaces. For a more exhaustive discussion, we refer the reader to an excellent review in [20].

Multidimensional decomposition techniques are used to extract underlying or latent features from a multidimensional array (an N -way tensor) \mathcal{X} . It should be recalled that a vector is said to be a tensor of mode one whereas a matrix is a tensor of mode two. A three-way tensor is a three-dimensional array having $I \times J \times K$ elements:

$$\mathcal{X} \in \mathbb{R}^{I \times J \times K} \quad (4)$$

$$\mathcal{X} = \mathbf{a} \circ \mathbf{b} \circ \mathbf{c} \quad (5)$$

The tensor rank decomposition decomposes a given tensor into a linear combination of rank-one tensors. A three-dimensional tensor is of rank-one, if it can be decomposed into the outer product of three vectors (refer to Equation 5). By analyzing each component of the rank-one tensor, it is possible to uncover hidden features in the original data. Therefore, these models are likewise utilized as a tool for blind source separation. One of the key advantages of a tensor decomposition is the uniqueness of its solution even under mild conditions. Other factorization methods require additional constraints such as statistical independence (independent component analysis) or orthogonality (singular value decomposition).

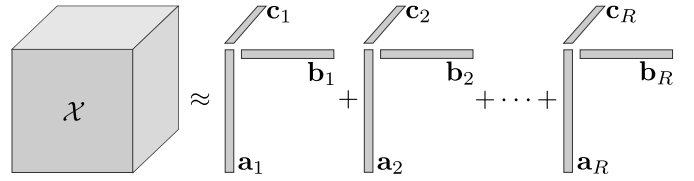


Fig. 2. The principle of canonical polyadic decomposition for a three-way tensor.

The canonical polyadic decomposition (CPD) is a tensor decomposition which was independently proposed by Carroll and Chang (known as CANDECOMP for canonical decomposition) [21] and Harshman (known as PARAFAC for parallel factors) [22]. Because of the similarity of the underlying principles, these approaches are known in the literature as CANDECOMP/PARAFAC or simply as canonical polyadic decomposition [20]. Their fundamental concept is to express a tensor as a sum of factorized rank-one tensors. For the three-way case this model results in the following representation:

$$\mathcal{X} \approx \sum_{r=1}^R \mathbf{a}_r \circ \mathbf{b}_r \circ \mathbf{c}_r \quad (6)$$

where R is a positive integer representing the number of rank-one components employed for the decomposition, also referred to as the decomposition rank. Figure 2 illustrates the principle of CPD. The tensor \mathcal{X} is decomposed into a sum of rank-one tensors. The resulting three-dimensional rank-one tensors consist of three loading vectors (\mathbf{a}_i , \mathbf{b}_i and \mathbf{c}_i) – each corresponding to one dimension of the decomposed tensor. These components can subsequently be used to extract latent information from \mathcal{X} . Similarly to SVD, each of the factors can then be the foundation for an exhaustive analysis of the data. Since we aim to extract motion artifacts from the ECG, our premise is to use tensor decomposition for blind source separation. We aim to separate noise and useful signal to different rank-one tensor in Eq. 6.

IV. APPLICATION OF TENSOR DECOMPOSITION

A. Data acquisition

In order to measure the electrocardiogram and physical exertions, we employed the *Shimmer3* platform [23]. The platform integrates, among others, a 3D accelerometer, a 3D gyroscope, and a 3D magnetometer as well as a 5-lead wireless ECG. Furthermore, the platform offers the possibility of sampling all the sensors synchronously. The ECG itself provides three bipolar leads through four input channels resulting in:

- Lead I (LA-RA): Left Arm - Right Arm
- Lead II (LL-RA): Left Leg - Right Arm
- Lead III (LL-LA): Left Leg - Left Arm

Shimmer provides two different accelerometer chips: a wide range (WR) accelerometer and a low noise (LN) accelerometer. While the LN accelerometer is capable of measuring fine-grained acceleration up to $\pm 2G$, the wide range accelerometer can be calibrated to measure accelerations in the

range of $\pm 8G$. This range is sufficient for all the activities we considered in our experiments. We placed the platform on the chest of a healthy adult subject, approximately three centimeters left of the sternum, central in the triangle formed by ECG leads I to III. From this position, the ECG electrodes extend in designated directions to measure cardiac action potentials whereas the inertial sensors dwell inside the platform. Hence, there is a displacement between the location where the electrodes measure the cardiac activity and the sensors recording the subject's motion. Consequently, the inertial measurements can be taken only as an approximation of the motion affecting the electrode.

To investigate the influence of motion on the electrocardiogram signal, we recorded a series of measurements at a rate of 512 samples per second while a healthy subject performed different types of physical exercises, namely, Push-Ups, Skipping, High-Knees, Single Jump, Running, Climbing up or down a flight of stairs at a normal pace, Climbing up or down a flight of stairs at a high speed, and biking. We analyzed the measurements to (1) examine the influence of motion on the ECG signal in general and (2) to compare the intensity of motion artifacts caused by the different activities. We observed that the ECG channels are affected by motion artifacts to a varying degree. While lead II is the least sensitive to motion, particularly lead I shows a high sensitivity to motion and similar interferences. In all the subsequent investigations we leave out the ECG measurements associated with lead II in order not to bias our observation.

B. Preprocessing

Figure 3 displays the raw data associated with a 120 s duration of skipping. The acceleration perpendicular to the ground (y-axis) shows the periodic motion performed, consisting of 10 s locomotion and 10 s resting. In addition to localized distortions, the ECG signal is also subject to a gradual drift in the baseline. This drift is caused by the motion as well as a gradual change in the electrical characteristics of the medium interfacing the electrodes with the skin. Since our main focus is on localized distortions, we first removed high-frequency noise and baseline wander using digital filters.

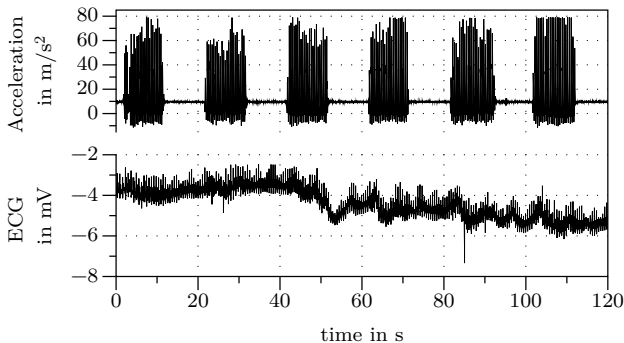


Fig. 3. Measurements taken from the y-axis of a 3D accelerometer and lead I (LA-RA) while the subject was skipping.

All signals were preprocessed using a low-pass filter with a cutoff frequency of $f_{c,low} = 150$ Hz and a high-pass filter with a cutoff frequency of $f_{h,high} = 0.5$ Hz. The cutoff frequencies are commonly used in clinical applications and considered to preserve the characteristics of the ECG in adults [24]. Subsequently, the 120 s of data were segmented into episodes of 30 s resulting in four segments for each activity. Other than that, the data were normalized using Equation 7 in order to avoid bias during the decomposition process:

$$x_{norm}(t) = \frac{x(t) - \min(x)}{\max(x) - \min(x)} \quad (7)$$

Data normalization is a common practice in multi-way data analysis, since it gives equal statistical significance to measurements originating from heterogeneous sources [17].

The row measurements describe the temporal aspects of cardiac and physical activities. Additional and complementary insights can be gained by examining their spectral aspects. Transformation techniques (such as Fourier Transformation) reveal spectral aspects, but in doing so, hide temporal aspects. For example, it is possible to detect a sudden surge in the heart rate using a Fourier Transform, but it is not possible to determine when this surge happens. Various approaches are conceivable to capture temporal and spectral aspects simultaneously, including Short-Time Fourier Transform (STFT) [25], and Wavelet Transformations (both discrete wavelet transform (DWT) and continuous wavelet transform (CWT) [26]).

In STFT, a time-series is segmented into multiple (and potentially overlapping) windows. In each window a Fast-Fourier Transform (FFT) is applied to determine the frequency components included in that specific window. The time and frequency resolutions depend on the size of the window. An improvement in the resolution of one of the dimensions inevitably results in a corresponding degradation in the resolution of the other dimension. For instance, fast-changing activities require short windows (high time resolution) to localise frequency changes, resulting in a low frequency resolution (because the observation period is short). By contrast, slow-changing activities require large observation windows to mark a change, resulting in a high frequency resolution but in a low temporal resolution.

Wavelet transformations use a base function Ψ , which is then stretched or compressed to capture low or high frequency components, respectively. The advantage of a wavelet transformation is the excellent time resolution for high frequencies while maintaining a high-frequency resolution for low frequencies. This makes a wavelet transformation suitable for capturing temporal and spectral aspects in our measurement sets. The wavelet transform has been applied extensively in the recent past for biomedical applications [16], [17]. Indeed, CWT and CPD have been applied to EEG data to extract artifacts and to differentiate between artifacts and seizures [17]. We employed CWT to transform the ECG data into time-frequency space. As a mother wavelet, we selected the Morlet wavelet [27].

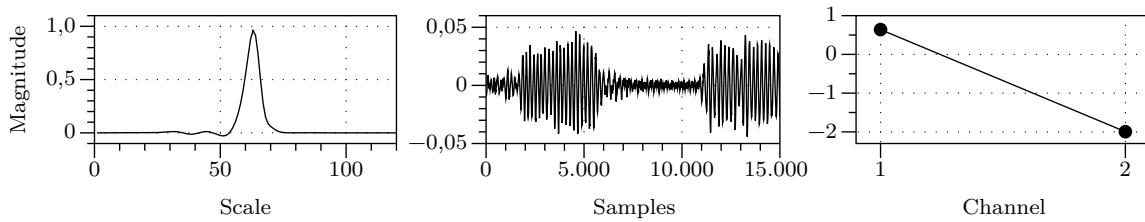


Fig. 4. The result of a rank five CPD for skipping, including the components for scale, time and channel.

C. Tensor Construction

Each channel of the wireless ECG generates a one-dimensional vector of size J , where J refers to the number of samples. We applied CWT to transform each vector into a two-dimensional frequency-time matrix of size $I \times J$, where I refers to the scaling factor of the mother wavelet and is inversely proportional to the frequency. By putting together the matrices of all the ECG channels in a multi-dimensional array, we produced a tensor of dimensions $I \times J \times K$ as can be visualized in Figure 5. The frontal slice of the tensor represents the wavelet transform of a single channel. It must be remarked at this point that the tensor was constructed using ECG signals only and no inertial measurement was included. The inertial measurements will be used to investigate how well the components of a decomposed tensor (the hidden features) are correlated with the actual physical movements.

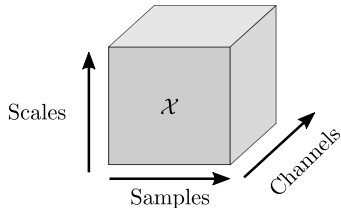


Fig. 5. Construction of the ECG tensor.

D. Tensor Decomposition

After the ECG tensor is constructed, we applied a five-component CPD model, as described in Equation 6. Each of the R components consists of three loading vectors, representing the three dimensions of our initial ECG tensor \mathcal{X} . Figure 4 displays the loading vectors for one component as a result of a CPD of rank five for running. Vector \mathbf{a} reveals the spectral properties of this component. The vector \mathbf{b} reveals the temporal aspects and the vector \mathbf{c} encodes how the ECG channels are associated with the hidden features. We used the *Tensorlab 3.0* Toolbox in *MATLAB* [28] to compute the tensor decomposition.

The premise for our attempt to uncover hidden features in a decomposed tensor is that motion artifacts are pervasive in all the ECG channels and manifest themselves more or less in a similar manner. This results in a three-dimensional correlation (i.e., temporal correlation, spectral correlation, and spatial correlation). An R -component tensor decomposition can take advantage of this correlation to highlight the underlying factors

which give rise to this correlation. By analyzing the factors, we can reason about the spectral composition of motion artifacts, their temporal characteristics, and their spatial distribution.

V. EVALUATION

The following section provides insight into the findings we obtained by decomposing ECG measurements using CPD.

A. Extraction of Motion Artifact using CPD

Figure 6 shows a comparison between the row data from the wide range accelerometer (y-axis, perpendicular to the ground), the ECG measurement of lead I (LA-RA) and one of the temporal CPD components (a result of the tensor decomposition). The ECG and the accelerometer data were collected while the subject was skipping. The accelerometer data reveal times of activity and resting. According to the experimental setup, the activity consists of periodic segments of ten seconds. Analyzing the data in detail shows the number of skips performed by counting the number of peaks in the accelerometer data. The electrocardiogram of lead I contains temporal episodes which are interfered by motion artifacts and episodes which can be declared as a clean signal. The CPD component features episodes of high magnitude (e.g. 22s to 30s) and episodes of low magnitude (e.g. 12s to 22s). These time segments coincide with the characteristics of the accelerometer. Similar observations were made for the activities push-ups and high-knees. This observation suggests that the CPD is able to extract the periodic motion patterns, which can be the causes of artifacts affecting the ECG signal.

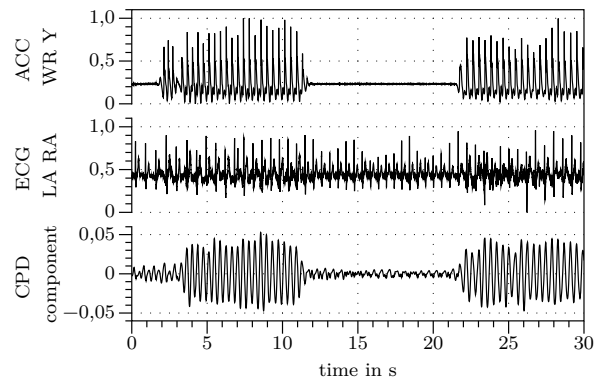


Fig. 6. Comparison of a wide range accelerometer, ECG lead I (LA-RA) and one CPD component extracted from data while a person was skipping.

We further investigated the extraction of artifacts for other modes of motion. Figure 7 displays a segment of data acquired while the subject was running. In contrast to skipping, push-ups and high-knees, where the subject periodically executed the activity, running was performed consistently for two minutes, reflecting everyday motion. As to the nature of the continuous activity, the tensor component does not show distinct episodes of activity. However, the tensor component can capture the start of running at around two seconds.

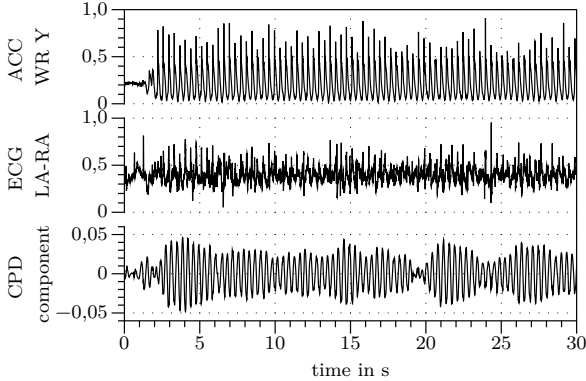


Fig. 7. Comparison of wide range accelerometer, ECG lead I (LA-RA) and one CPD component extracted from data while a person was running.

In Figure 8 a comparison between the accelerometer data and the CPD component, representing motion induced artifacts, is displayed for an arbitrarily selected interval of five seconds of running. We investigated the correlation between both time series. The accelerometer data contains distinct maxima, which likely occurred immediately after the subject’s foot touched the ground and the body accelerated to initiate forward movement. These maxima coincide with the minima in the CPD component. While the maxima of the accelerometer data exhibit spiky characteristics with a high gradient, the minima of the CPD component are flatter. However, the overlapping maxima and minima respectively prove that tensor decomposition is capable of extracting motion artifacts. Since we only included ECG data into our decomposition, the source of the motion patterns extracted must be the artifacts present in the ECG signal. The temporal correlation between both signals indicates that these artifacts were indeed caused by movement.

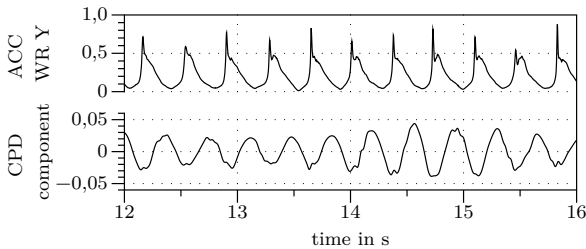


Fig. 8. Comparison of a CPD component and the measurement obtained by one of the axes of a 3D accelerometer for an arbitrarily selected five seconds interval of running.

Using a Fast-Fourier Transformation (FFT) we analyzed both signals regarding their frequency components. The maximum of both signals overlaps at a frequency of 2.7 Hz. From that, we can calculate the cadence of the runner, which is around 160 steps per minute. The average for moderately trained athletes is around 160 to 180 steps per minute indicating that our results are indeed plausible.

To study the correlation between extracted artifacts and inertial data, we employed the Pearson correlation coefficient on all sensor combinations. Table I displays the maximum of the absolute correlation coefficients between CPD components and the respective inertial sensors. The ECG was segmented in 30 s intervals and for each interval, a CPD was performed. All temporal loading vectors, resulting from CPD, were correlated with the inertial sensors for the respective time segment. The values within the Table represent the maximum of the absolute correlation coefficient. In our analysis we noted that the sign of the CPD components is not subject to a distinct set pattern. Hence, we only considered the absolute values of correlation.

The correlation coefficients of wide range and low noise accelerometer are almost identical, with deviations of a maximum of $\Delta R = 0.03$. Since the low noise accelerometer is limited to an acceleration of 2G and some activities exceed this threshold by more than 4G (e.g., skipping, running), the data shows segments of sensor saturation. Hence, we left out the low noise accelerometer from the Table and further considerations.

TABLE I
ABSOLUTE CORRELATION BETWEEN CPD COMPONENT AND INERTIAL SENSORS FOR THE ACTIVITIES PERFORMED.

	Gyroscope			Accelerometer WR		
	X	Y	Z	X	Y	Z
Running	0.63	0.51	0.41	0.51	0.71	0.50
High-Knees	0.22	0.18	0.40	0.08	0.50	0.33
Skipping	0.28	0.25	0.34	0.04	0.50	0.50
Stairs fast	0.19	0.19	0.27	0.25	0.51	0.14
Stairs normal	0.07	0.06	0.05	0.05	0.42	0.23
Push-Ups	0.05	0.13	0.06	0.11	0.04	0.03
Bike	0.13	0.19	0.20	0.25	0.16	0.14
Single Jump	0.06	0.07	0.07	0.04	0.18	0.09

The correlation between a tensor component and inertial data is heavily dependent on two factors: (1) Mode of motion and (2) Axis of inertial measurement. As regards (1), the mode of motion strongly affects the intensity of artifacts present in the ECG. Figure 9 displays the ECG lead I of the two activities skipping and single jumps. It is clear that the ECG signal obtained from single jumps is less noisy than that from skipping. This suggests that the reason for a low correlation between inertial measurements and CPD components can be a low noise ECG signal. Concerning (2), the strength of correlation also varies across the different inertial axes. The reason for this might be the different intensities of the movement on the orthogonal axes. Running contains forward, sideways and upward components and thus induces motion artifacts which correlate to the respective axis. Sideways motion in skipping

is however limited in its intensity, resulting in fewer artifacts and hence the inertial data are weakly correlated.

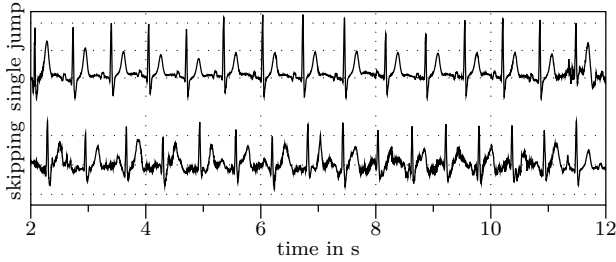


Fig. 9. Comparison of ECG lead I (LA-RA) for the activities single jump and skipping.

On the other hand, low correlation values ($R \leq 0.29$) are present for significantly disturbed ECG. As shown in Figure 10, biking induces a good portion of noise in the signal. However, the correlation between the CPD component and inertial data is low ($R_{max} = 0.25$). The reason might be the origin of the motion artifacts. During earlier experiments, the authors noticed that moving or touching the electrodes induces artifacts, which highly distort the ECG to a point where no QRS-Detection is possible. While running and skipping have distinct patterns of lateral acceleration perpendicular to the ground, the sources of artifacts for biking might be manifold – such as clothes touching the ECG cables and adhesive electrodes, which, due to their origin, are not correlated to inertial measurements. In addition, the ECG signal might be superimposed by electromyogram (EMG) contents (action potentials generated by the contraction and relaxation of muscles). In contrast to running and skipping, where most motion is generated by leg muscles, biking also involves pectoral muscles in order to lean on the handlebar. The ECG electrodes placed on the thorax might capture not only cardiac activity but also the potential change induced by pectoral muscle groups.

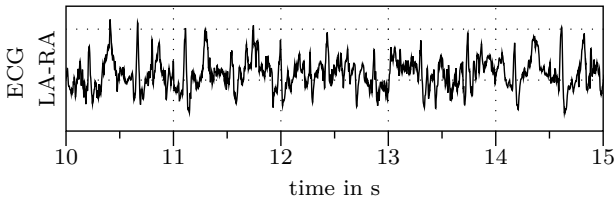


Fig. 10. Measurements of lead I (LA-RA) ECG while the subject was biking subject with presence of noise

In order to verify our findings and prove that the correlation is not solely based on the correlation between ECG and inertial measurements, we provide Table II. We, therefore, employed Pearson’s correlation between the ECG channels used for CPD and the inertial sensors for the respective time segments. As for the CPD case, we only considered the absolute values of correlation. Thus, $R_{ecg,inert}$ is determined by calculating the correlation coefficient between all ECG channels and inertial data. Then we took the absolute values of these and

determined the maximum value for all time segments of one activity. $R_{cpd,inert}$ is the correlation coefficient between the temporal CPD component and the respective inertial sensors, as displayed in Table I. The difference between both is then as follows:

$$R_{diff} = R_{cpd,inert} - R_{ecg,inert} \quad (8)$$

As Table II shows, CPD components have stronger or almost equal correlation values than the ECG. Indeed, CPD is capable of establishing a stronger correlation than ECG itself, improving R_{corr} up to 0.41 for acceleration in the x-axis while running. If the ECG has higher correlation coefficients, the differences are within a margin of $\Delta R \leq 0.11$ and usually for activities and sensors for which CPD could not establish correlation values of $R \geq 0.29$. Hence, we consider these to be negligible. However, we can conclude, that CPD is capable of improving the correlation for most of the activities performed and moreover, can extract temporal patterns of motion.

TABLE II
DIFFERENCE BETWEEN ABSOLUTE CORRELATION OF CPD VS. INERTIAL SENSORS AND ECG VS. INERTIAL SENSORS

	Gyroscope			Accelerometer WR		
	X	Y	Z	X	Y	Z
Running	0.15	0.17	-0.10	0.41	0.19	0.13
High-Knees	0.15	0.10	0.24	0.03	0.30	0.19
Skipping	0.22	0.19	0.28	-0.02	0.31	0.31
Stairs fast	0.07	-0.04	0.02	0.08	0.21	0.05
Stairs normal	-0.07	-0.08	-0.02	-0.07	0.22	0.05
Push-Ups	-0.04	-0.04	-0.02	0.04	-0.03	-0.10
Bike	-0.02	-0.11	0.02	0.04	0.03	-0.01
Single Jump	-0.03	0.01	-0.04	0.01	0.04	0.02

VI. CONCLUSION AND FUTURE WORK

In this paper, we employed canonical polyadic decomposition to extract motion artifacts from the measurements of a wireless electrocardiogram. We took measurements from a healthy subject undertaking different types of movements associated with everyday activities. Using a the *Shimmer3* platform we simultaneously acquired the data from a 3D accelerometer, a 3D gyroscope and a five lead ECG. We constructed a three-way tensor consisting of the dimensions time, scale and channel and employed canonical polyadic decomposition in order to uncover hidden features in the original data. The extracted components were subsequently analyzed for their correlation to the motion patterns performed by considering the measurement sets of the inertial sensors.

Our initial results suggest that CPD is capable of extracting motion artifacts from the ECG data without the need for any constraints. Depending on the mode of motion, CPD extracted temporal factors exhibiting a high correlation to inertial data. Especially motion generated by repetitive acceleration patterns, such as running, skipping and high-knees, shows high correlation coefficients. Although biking and performing push-ups yield to a high degree of artifacts in the ECG, the CPD did not yield in an increase of the correlation coefficients.

The reasons might be manifold, but our evaluation suggests that the electric muscle activity could superimpose the ECG. Nevertheless, CPD was successful in extracting motion artifacts from ECG signals.

In future research, the authors intend to further investigate the correlation between electrocardiogram and motion artifacts. Tensor decomposition represents a powerful tool to fuse data collected by multiple sensor sources. Our initial approach limits the tensor construction to ECG data exclusively. Increasing the tensor dimensions by using additional data sources (e.g. EMG, accelerometer, gyroscope) might provide insights into the motion artifact statistics to a greater extent. Advanced tensor decompositions such as Tucker or higher-order singular value decomposition (refer to [20]) could furthermore enhance the extraction of artifacts and might be used to reduce the motion artifacts present in wireless electrocardiograms.

REFERENCES

- [1] World Health Organization, "World Health Statistics 2016: Monitoring health for the SDGs," World Health Organization, Tech. Rep., 2016.
- [2] B. Yu, L. Xu, and Y. Li, "Bluetooth Low Energy (BLE) based mobile electrocardiogram monitoring system," *2012 IEEE International Conference on Information and Automation, ICIA 2012*, no. June, pp. 763–767, 2012.
- [3] A. Alzaidi, L. Zhang, and H. Bajwa, "Smart textiles based wireless ECG system," *2012 IEEE Long Island Systems, Applications and Technology Conference, LISAT 2012*, pp. 1–5, 2012.
- [4] R. Gupta and M. Mitra, "Wireless Electrocardiogram Transmission in ISM Band: An Approach Towards Telecardiology," *Journal of Medical Systems*, vol. 38, no. 10, 2014.
- [5] Y. D. Lee and W. Y. Chung, "Wireless sensor network based wearable smart shirt for ubiquitous health and activity monitoring," *Sensors and Actuators, B: Chemical*, vol. 140, no. 2, pp. 390–395, 2009.
- [6] S. Y. Lee, J. H. Hong, C. H. Hsieh, M. C. Liang, S. Y. C. Chien, and K. H. Lin, "Low-power wireless ECG acquisition and classification system for body sensor networks," *IEEE Journal of Biomedical and Health Informatics*, vol. 19, no. 1, pp. 236–246, 2015.
- [7] N. V. Thakor, J. G. Webster, and W. J. Tompkins, "Estimation of QRS Complex Power Spectra for Design of a QRS Filter," *IEEE Transactions on Biomedical Engineering*, vol. BME-31, no. 11, pp. 702–706, nov 1984.
- [8] M. Milanese, N. Martini, N. Vanello, V. Positano, M. F. Santarelli, and L. Landini, "Independent component analysis applied to the removal of motion artifacts from electrocardiographic signals," *Medical and Biological Engineering and Computing*, vol. 46, no. 3, pp. 251–261, mar 2008.
- [9] P. Mishra and S. K. Singla, "Artifact removal from biosignal using fixed point ICA algorithm for pre-processing in biometric recognition," *Measurement Science Review*, vol. 13, no. 1, pp. 7–11, 2013.
- [10] S.-H. Liu, "Motion Artifact Reduction in Electrocardiogram Using Adaptive Filter," *Journal of Medical and Biological Engineering*, vol. 31, no. 1, p. 67, 2011.
- [11] H. Kim, S. Kim, N. Van Helleputte, T. Berset, D. Geng, I. Romero, J. Penders, C. Van Hoof, and R. F. Yazicioglu, "Motion artifact removal using cascade adaptive filtering for ambulatory ECG monitoring system," *2012 IEEE Biomedical Circuits and Systems Conference: Intelligent Biomedical Electronics and Systems for Better Life and Better Environment, BioCAS 2012 - Conference Publications*, pp. 160–163, 2012.
- [12] M. Kirst, B. Glauner, and J. Ottenbacher, "Using DWT for ECG motion artifact reduction with noise-correlating signals," *Proceedings of the Annual International Conference of the IEEE Engineering in Medicine and Biology Society, EMBS*, pp. 4804–4807, 2011.
- [13] P. Mithun, P. C. Pandey, T. Sebastian, P. Mishra, and V. K. Pandey, "A wavelet based technique for suppression of EMG noise and motion artifact in ambulatory ECG," *Proceedings of the Annual International Conference of the IEEE Engineering in Medicine and Biology Society, EMBS*, pp. 7087–7090, 2011.
- [14] I. Romero, "PCA and ICA applied to noise reduction in multi-lead ECG," *2011 Computing in Cardiology (CinC)*, pp. 613–616, 2011.
- [15] S. Pongponsoi and X. H. Yu, "An adaptive filtering approach for electrocardiogram (ECG) signal noise reduction using neural networks," *Neurocomputing*, vol. 117, pp. 206–213, 2013.
- [16] J. E. Kline, H. J. Huang, K. L. Snyder, and D. P. Ferris, "Isolating gait-related movement artifacts in electroencephalography during human walking," *Journal of Neural Engineering*, vol. 12, no. 4, 2015.
- [17] E. Acar, C. Aykut-Bingol, H. Bingol, R. Bro, and B. Yener, "Multiway analysis of epilepsy tensors," *Bioinformatics*, vol. 23, no. 13, pp. 10–18, 2007.
- [18] W. Dargie, "Motion Artefacts Modelling in the Application of a Wireless Electrocardiogram," in *2018 21st International Conference on Information Fusion (FUSION)*, no. May. IEEE, jul 2018, pp. 239–244.
- [19] L. Billiet, T. Swinnen, K. de Vlam, R. Westhovens, and S. Van Huffel, "Recognition of Physical Activities from a Single Arm-Worn Accelerometer: A Multiway Approach," *Informatics*, vol. 5, no. 2, p. 20, apr 2018.
- [20] T. G. Kolda and B. W. Bader, "Tensor Decompositions and Applications," *SIAM Review*, vol. 51, no. 3, pp. 455–500, aug 2009.
- [21] J. D. Carroll and J.-J. Chang, "Analysis of individual differences in multidimensional scaling via an n-way generalization of Eckart-Young decomposition," *Psychometrika*, vol. 35, no. 3, pp. 283–319, sep 1970.
- [22] R. A. Harshman, "Foundations of the PARAFAC Procedure: Models and Conditions for an Explanatory Multimodal Factor Analysis," vol. 35, no. 3, pp. 283–319, 1970.
- [23] A. Burns, B. R. Greene, M. J. McGrath, T. J. O'Shea, B. Kuris, S. M. Ayer, F. Strojescu, and V. Cionca, "SHIMMER A Wireless Sensor Platform for Noninvasive Biomedical Research," *IEEE Sensors Journal*, vol. 10, no. 9, pp. 1527–1534, sep 2010.
- [24] P. Kligfield, L. S. Gettes, J. J. Bailey, R. Childers, B. J. Deal, E. W. Hancock, G. van Herpen, J. A. Kors, P. Macfarlane, D. M. Mirvis, O. Pahlm, P. Rautaharju, and G. S. Wagner, "Recommendations for the Standardization and Interpretation of the Electrocardiogram," *Circulation*, vol. 115, no. 10, pp. 1306–1324, 2007.
- [25] J. Allen, "Short term spectral analysis, synthesis, and modification by discrete Fourier transform," *IEEE Transactions on Acoustics, Speech, and Signal Processing*, vol. 25, no. 3, pp. 235–238, jun 1977.
- [26] C. E. Heil and D. F. Walnut, "Continuous and Discrete Wavelet Transforms," *SIAM Review*, vol. 31, no. 4, pp. 628–666, dec 1989.
- [27] D. Morlet, F. Peyrin, P. Desseigne, P. Touboul, and P. Rubel, "Time-scale analysis of high-resolution signal-averaged surface ECG using wavelet transformation," in *Proceedings Computers in Cardiology*. IEEE Comput. Soc. Press, 1991, pp. 393–396.
- [28] N. Vervliet, O. Debals, L. Sorber, M. Van Barel, and L. De Lathauwer, "Tensorlab 3.0," 2016. [Online]. Available: <https://www.tensorlab.net>